A Modification to the NOAH LSM to Simulate Heat Mitigation Strategies in the New York City Metropolitan Area

BARRY H. LYNN,*,+ TOBY N. CARLSON,# CYNTHIA ROSENZWEIG,@ RICHARD GOLDBERG,* LEONARD DRUYAN,* JENNIFER COX,& STUART GAFFIN,* LILY PARSHALL,* AND KEVIN CIVEROLO**

*Center for Climate Systems Research, Columbia University, New York, New York
#Department of Meteorology, The Pennsylvania State University, University Park, Pennsylvania
@NASA Goddard Institute for Space Studies, and Center for Climate Systems Research, Columbia University, New York, New York
&Hunter College of the City University of New York, New York, New York
**Bureau of Air Research, New York State Department of Environmental Conservation, Albany, New York

(Manuscript received 7 May 2007, in final form 2 June 2008)

ABSTRACT

A new approach to simulating the urban environment with a mesocale model has been developed to identify efficient strategies for mitigating increases in surface air temperatures associated with the urban heat island (UHI). A key step in this process is to define a ''global'' roughness for the cityscape and to use this roughness to diagnose 10-m temperature, moisture, and winds within an atmospheric model. This information is used to calculate local exchange coefficients for different city surface types (each with their own ''local roughness'' lengths); each surface's energy balances, including surface air temperatures, humidity, and wind, are then readily obtained. The model was run for several summer days in 2001 for the New York City five-county area. The most effective strategy to reduce the surface radiometric and 2-m surface air temperatures was to increase the albedo of the city (impervious) surfaces. However, this caused increased thermal stress at street level, especially noontime thermal stress. As an alternative, the planting of trees reduced the UHI's adverse effects of high temperatures and also reduced noontime thermal stress on city residents (and would also have reduced cooling energy requirements of small structures). Taking these results together, the analysis suggests that the best mitigation strategy is planting trees at street level and increasing the reflectivity of roofs.

1. Introduction

High-density metropolitan areas are known for their ''urban heat island'' (UHI) effect that raises nighttime temperatures in dense cityscapes in response to daytime heating of city surfaces. During sunny daytime hours, reduced evaporation of city surfaces coupled with the thermal properties of the city building and paving materials (e.g., Myrup 1969; Kunkel et al. 1996; Roberts et al. 2006; Kusaka and Kimura 2004) allows the cityscape to absorb heat, which is then emitted at night as longwave radiation. This radiation emitted at night combines with anthropogenic heating (e.g., Livezey and Tinker 1996; Sailor and Fan 2004; Coutts et al. 2007) to raise nighttime temperatures in urban ''canyons'' relative to surrounding rural areas.

When the UHI exists along the coast, Ohashi and Kida (2002) note that high temperatures in cities such as New York can enhance the development of sea-breeze circulations. Changes in the sea-breeze circulation (or city–rural breezes) due to the UHI can impact temperatures and pollution dispersion within cities themselves. Green-up of planted areas within urban areas can also lead to within-urban differences in surface temperatures (Chen et al. 2003; Gallo et al. 1993) and very localized breezes. Temperature differences between the city core and rural outlying areas can also lead to the development of localized mesoscale circulations.

Bornstein (1968) observed the occurrence of the

+ Current affiliation: Weather It is, Ltd., Efrat, Israel.

Corresponding author address: Dr. Barry H. Lynn, Center for Climate Systems Research, 2880 Broadway, New York, NY 10025.
E-mail: barry-lynn@weather-it-is.com

DOI: 10.1175/2008JAMC1774.1

© 2009 American Meteorological Society

UHI effect in New York City (NYC). He measured a maximum in air temperature differences near the surface late at night, with the difference between the city air temperature and its surroundings usually decreasing with height up to about 300 m, where it was no longer observable. Balling and Cerveny (1987) observed a long-term association between the development of the Phoenix, Arizona, UHI and an increase in early morning wind speeds. They suggested that the increase in wind speed was due to a decrease in nighttime stability associated with the nighttime urban heat island. Hawkins et al. (2004) deployed a dense network of temperature and humidity sensors across different land uses on an agricultural farm southeast of Phoenix for a 10-day period in April of 2002. Temperature data from these sensors were compared with data from Sky Harbor Airport in Phoenix (an urban station), and the smallest and largest nighttime temperature differences between locations on the farm at a given time were 0.8° and 5.4°C, respectively. Depending on the choice of rural baselines, the average and maximum urban heat island effects ranged from 9.4° to 12.9°C and from 10.7° to 14.6°C. Kim and Baik (2002) investigated the maximum UHI intensity in Seoul, South Korea, using data measured at two meteorological observatories (an urban site and a rural site) during the period of 1973–96. The average maximum UHI was weakest in summer and strongest in autumn and winter. It increased over this time period from about 3° to 3.5°C. Similar to previous studies for other cities, the maximum UHI intensity was more frequently observed in the nighttime than in the daytime, decreased with increasing wind speed, and was more pronounced during clear skies. Ackerman (1985) also found that the impact of the UHI varies seasonally as well as diurnally (modified by cloud and wind direction). Kunkel et al. (1996) found that the UHI raised nocturnal surface temperatures in the city of Chicago, Illinois, during the 1995 heat wave by more than 2°C. Extreme temperatures coupled with high dewpoints and high pollution levels contained within a shallow boundary layer exacerbated the impacts of the heat wave on human health, leading to many deaths.

Zehnder (2002) highlighted problems with using the fifth-generation Pennsylvania State University–National Center for Atmospheric Research Mesoscale Model (MM5) (Dudhia 1993; Grell et al. 1994; Chen and Dudhia 2001a,b) to simulate the UHI in Phoenix. The MM5 with a five-layer slab model underestimated the magnitude of the diurnal temperature maximum and also caused the maximum to occur too early in the day. They attributed this problem to an overestimation of latent heat fluxes within the city surface. They found that adjusting the soil moisture of the urban (and shrub) areas from 10% to 0% improved the modeled maximum temperatures but that the model temperatures were too cool at night because the model did not, for example, simulate realistically urban heat storage or include ''urban canopy'' terms (e.g., a heat capacity that includes the contribution from walls, a smaller sky-view factor, shadow and trapping of radiation between buildings, and heating from rooftops).

Taha (1999) modified a simple bulk parameterization scheme to include an urban heat storage term in the surface energy balance terms. This raised simulated temperatures in the Atlanta, Georgia, city area by about 1.5°C. Grossman-Clarke et al. (2005) refined the land cover classification for the arid Phoenix metropolitan area and added some simple modifications to the surface energetics of MM5. The single urban category in the existing 24-category U.S. Geological Survey land cover classification used in MM5 was divided into three classes to account for heterogeneity of urban land cover. They then used bulk approaches to characterize further the urban surface energy budget, such as heat storage, the production of anthropogenic heat, and radiation trapping within the five-layer slab model. The new land surface classification scheme had a significant impact on the turbulent heat fluxes and the evolution of the boundary layer, which improved the capability of MM5 to simulate the daytime part of the diurnal temperature cycle in the urban area. Likewise, the inclusion of radiation trapping, heat storage, and anthropogenic heating significantly improved the simulation of nighttime near-surface air temperatures.

More recent efforts have been directed at simulating the more detailed impacts of urban architecture on the UHI. For instance, Otte et al. (2004), Dupont et al. (2004), and Chin et al. (2005) have all developed urban canopy models. Kusaka et al. (2005) implemented an urban canopy model in the Weather Research and Forecasting Model (WRF). In an idealized test case, they found that the nocturnal heat island was better simulated because their model accounted for anthropogenic heating and urban canyon structure. Holt and Pullen (2007) produced high-resolution numerical simulations using the Coupled Ocean–Atmosphere Mesoscale Prediction System with the WRF urban canopy model for a 23-day period in August of 2005 for the NYC metropolitan area. They showed that the combined model simulated well the nocturnal urban heat island, with only a very small bias at night when heating from anthropogenic sources were accounted for to simulate correctly the nocturnal heat island.

Huang et al. (1987) suggest that increasing vegetation cover in cities can reduce the amplitude of the UHI and lessen summer air conditioning requirements. Taha

(1996) investigated the impact of increased vegetation on ozone air quality, and Taha (1997) suggested that high-albedo surfaces should be part of new city codes to reduce surface cooling requirements. Civerolo et al. (2000) and Nowak et al. (2000) combined MM5 with a soil model to study the effect of increasing the potential evaporation on urban temperatures. They suggested that surface mitigation strategies could be an important way to reduce heat-wave impacts on city populations that are exacerbated by, for example, elevated surface temperature associated with solar heating of the surface layer in built-up areas. Such heating can also affect other characteristics of the UHI, such as boundary layer heights and boundary layer mixing.

The National Centers for Environmental Prediction–Oregon State University–Air Force–Hydrologic Research Laboratory (Noah) land surface model (LSM) (Liu et al. 2006) was recently upgraded to account for urban properties on urban temperatures, but using a less sophisticated approach than that described in Kusaka et al. (2005). We describe a further modification to the Noah LSM implementation, which involves the development of a simultaneous energy balance model (SEBM). The purpose is to use the modified model to study the potential for mitigation of the UHI of the NYC five-county area, but we also explore strategies for mitigating the effects of an urban environment on the radiative heat stress perceived by an individual at street level during the time of maximum solar heating (noontime). A secondary feature of these simulations is to illustrate the use of a new surface layer formulation that allows one to specify the urban canyon and its geometry as well as the heat balance at street level in the interstitial spaces between buildings. The strategies to be employed are planting trees on grass and streets, and increasing the albedo of impervious surfaces (streets/rooftop). The mitigation strategies will evaluate the effect of mitigation on surface radiometric and 2-m temperatures, as well as a measure of the effective temperature experienced by a person at street level standing under a tree, on an unsheltered grassy surface, or on an unsheltered impervious surface at noontime.

2. Methods

Seguin and Gignoux (1974) conducted a field experiment in France for the purpose of evaluating the effects of wind stress on crops planted between hedges. The hedgerows were removed to increase the wind stress on the crops. They showed that the presence of the hedgerows created two turbulent regimes, one responsive to the taller vegetation (the hedgerows) and the other responsive to the crops or grass in between. The one regime, existing above the level of the trees, exhibited a logarithmic wind profile with a roughness length characteristic of the trees. Below the tops of the trees and the shorter vegetation between the hedges, the logarithmic wind profile behaved as if the roughness length were that of the shorter vegetation. The upper regime can be said to have a ''global'' roughness length—one appropriate to the taller vegetation. A ''local'' roughness length appears to be appropriate to describe the turbulent regime associated with the shorter vegetation.

We propose to extend the findings of Seguin and Gignoux to the urban canopy. In so doing, we are implementing an idea first proposed by Oke (1976) and discussed in Arnfield's (2003) review on the UHI. They refer to an ''urban canopy layer'' and an ''urban boundary layer,'' whereby the buildings of a cityscape (with its global roughness length) obstruct the flow of air to the underlying surfaces, such that different turbulent regimes can develop between the buildings above different surfaces (e.g., pavements, grass, and trees), each with its own smaller local roughness lengths and site-specific turbulent heat fluxes. By extension, the logarithmic wind profile between the top of the surface layer and the tops of the buildings differs from the logarithmic wind profile that extends from the tops of the buildings to the underlying surfaces between buildings; the logarithmic wind profiles are shown schematically in Fig. 1. Hence, we will define two roughness regimes for each grid point in the model, a global one appropriate to buildings and a local one appropriate to a tree-covered surface, a grass surface, or bare surfaces (including city streets and sidewalks). Following Seguin and Gignoux, we assume that the global roughness length applies to the buildings and governs the regime above the rooftop level while the local roughness length governs the wind profile between the top of the buildings and the surface. The two regimes join at an elevation representative of the buildings' tops (e.g., 10 m in our invented urban surface).

In the mesoscale model, the global logarithmic wind profile varies from the wind speed at the top of the surface layer (e.g., 35 m), where the roughness length is appropriate to the assumed building heights (e.g., 0.8 m). In the lower regime, the wind profile extends from the value of the wind speed at building level to the surface, as dictated by the lower roughness length. The upper regime, however, is not independent of the lower one, being indirectly linked via feedback from the surface sensible heat flux at ground level.

The assumption that buildings will respond like trees and the fact that the wind may blow at any angle to the rows of buildings may stretch the results of Seguin and Gignoux, but in the absence of contradictory data we

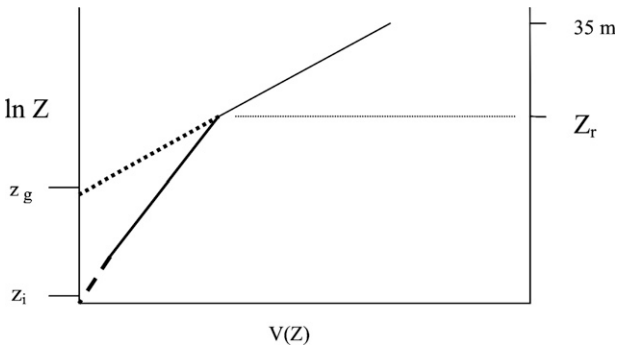

FIG. 1. Schematic semilog profile illustrating the dual roughness length regime. The vertical profile of the wind speed is plotted as a function of the logarithm of height Z and the wind speed V in the surface layer below 35 m. From 35 m to the height of the roof tops Z_r, the profile is a straight line whose projection along the dotted line to $V = 0$ (the global roughness height) is Z_g. Global roughness is assigned one value for each grid point appropriate to the buildings. Below the tops of the buildings, the wind profile responds to the interstitial surfaces between the buildings (grass, trees, and pavement), whose roughness lengths are smaller than for the buildings and whose slopes are therefore steeper (e.g., the heavy solid line). The projection of the heavy solid line to zero wind speed (dashed-line extension) defines a local roughness length Z_i, the latter applying to points within the grid box by the height of grass, trees, and paved obstacles at ground level.

believe this is a reasonable approach when simulating the cityscape with a mesoscale model.

a. Modification of the mesoscale model

Figure 2 illustrates how we applied the global and local approach to a cityscape within a mesocale model (here, the mesoscale model system is MM5; Dudhia 1993; Grell et al. 1994). The surface types of the cityscape are defined here as impervious, grass, and tree. Water surfaces are also considered because NYC and vicinity include bodies of water. The surface characteristics (e.g., albedo and roughness length) are defined in Table 1, and values of roughness length for trees are consistent with those of orchards (Pielke 1984). Within any single grid element of MM5 these surfaces can exist in varying proportions. In any model time step, the surface energy balances for each surface are calculated at the same time, and this approach is referred to as a SEBM (defined above).

To calculate local exchange coefficients for each surface requires that we define the lower boundary of the global roughness regime as related to the global roughness length Z_g, which applies to the log-linear profile from the nominal top of the surface layer at 35 m to the top of the buildings at Z_r (Fig. 1). We then use a global exchange coefficient derived from similarity relationships based on the mesoscale model's first-level prognosticated variables to diagnose the 10-m temperature, moisture, and wind (as illustrated in Fig. 2). The diagnosed variables are then used with each surface's local roughness length Z_i to obtain surface heat fluxes from each. An aggregate of the heat fluxes over each grid element is computed from the various surfaces. It is composed of contributing fluxes derived from individual surface layer wind profiles. This aggregate is directly coupled with the model first-level temperature and winds. Hence, SEBM's aggregate fluxes are used to calculate the tendencies of temperature, moisture, and wind in the first layer of the atmospheric model. Yet, each surface's local energy balance is indirectly affected by other surfaces within the same individual grid box via feedbacks with the model's first-layer prognostic variables.

The calculation of the surface energy balances for the different city surfaces was based on the Noah LSM in MM5 (Chen and Dudhia 2001a,b), as modified by Liu et al. (2006) for an urban environment. The LSM is a single canopy layer, in which the canopy layer shades the ground surface from direct solar radiation. The evaporation from the ground surface is proportional to the potential evaporation of the ground surface times the quantity 1 minus the vegetation fraction, where the proportionality of the relationship depends on the available soil moisture (so the evaporation from an impervious surface would be negligible). Instead of implementing more advanced and computer-intensive urban architecture, Liu et al. (2006) modified the model land surface parameters to represent more accurately the urban environment (here, referred to as LSUM). The LSUM surface albedo was reduced from 0.18 to 0.15; this reduction accounted for the shortwave radiation trapping in the urban canyons. The volumetric heat capacity was increased to 3.0×10^6 J m^{-3} K^{-1}, and the soil thermal conductivity was increased to 3.24 W m^{-1} K^{-1}. These two values are larger than those for the prevailing concrete/asphalt materials (about 2.0×10^6 J m^{-3} K^{-1} and 2.0 W m^{-1} K^{-1}, respectively) to roughly reflect the heat storage resulting from building walls. Last, the green vegetation fraction was reduced to 0.05, and the available urban soil water capacity was decreased to reduce evaporation. At present, there is no proper estimate of the bulk water capacity in urban regions. These were adjusted to keep the surface latent heat flux small when there is no rain. It appears that first-order effects of the urban architecture on the model simulation of urban surface layer temperatures (within a high-resolution mesoscale model) can be represented reasonably well with simple treatments of the land surface that do not include more advanced urban canopy models noted above.

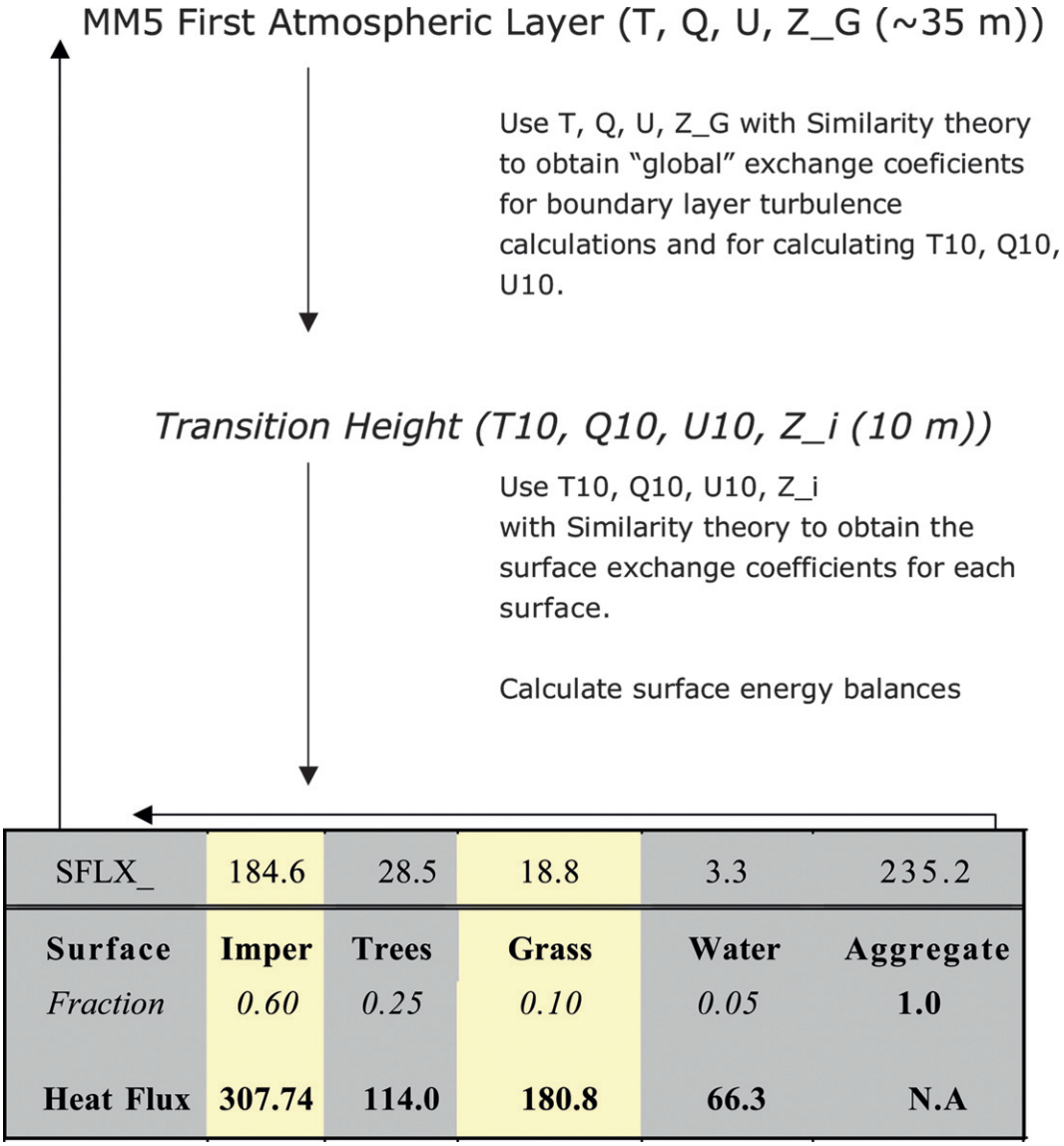

FIG. 2. Illustration of how SEBM is used in a mesocale model to calculate surface heat fluxes and surface temperatures. SFLX (top row, column six) is the aggregate flux weighted by the fractional contribution of each surface (top row, columns 2–5). The units of all heat fluxes are watts per meter squared.

To apply the changes made in the Noah LSM as detailed in Figs. 1 and 2 and to develop the SEBM used here to study mitigation impacts, further modifications were made to LSUM. For instance, program arrays for four different surface types were defined in the model code. Arrays for local exchange coefficients were also created that were dependent on 10-m temperatures, winds, and humidity (which were assumed to be at the

TABLE 1. Surface characteristics in MM5.

Land use type	Leaf area index	Vegetation fraction	Min canopy resistance (s m^{-1})	Shortwave albedo (%)	Longwave emissivity (%)	Roughness length (cm)	Initial soil moisture (vol/vol)
Trees (deciduous)	6	0.9	100	16	93	50	All layers at 90% saturation
Grass	1	0.5	40	19	98.5	12	Top layer at 50% saturation; other layers at 90%
Impervious	0.0	0.0	—	15	88	5	All layers "desiccated"

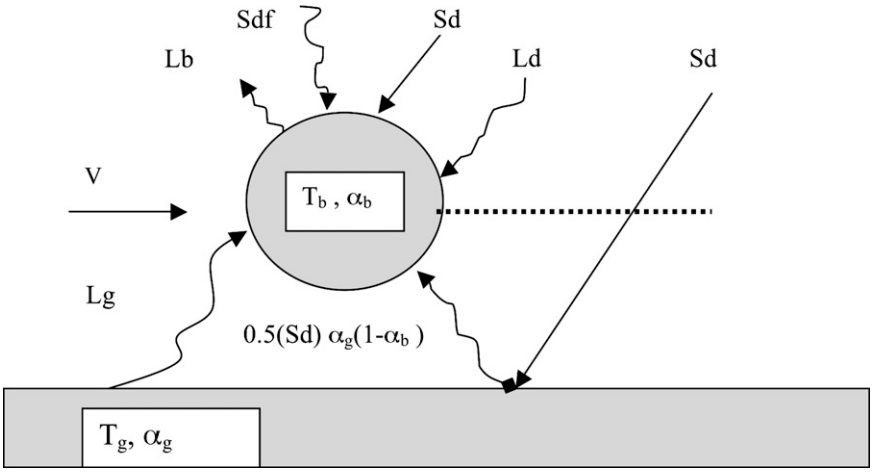

FIG. 3. Energy balance on a hypothetical sphere representing a bare, uncovered head. The various energy components expressed by Eq. (2) in the text are labeled: the downward incident direct solar flux S_d, the diffuse solar flux S_{df} (assumed to affect both sides of the sphere equally), the downward longwave flux L_d, the upward longwave flux emitted from the surface L_g, the longwave flux from the body L_b, and the reflected solar component from the ground, whose properties are surface temperature T_g and surface reflectance α_g. The surface temperature of the body is T_b, and its reflectance is α_b. The ambient wind speed is V. The horizontal dotted line represents the midpoint of the sphere, below which the upward energy components impinge on the lower half of the sphere. In this paper, the time-dependent variables are Sd and T_g. Ground reflectance α_g is changed in one simulation to illustrate the effect of artificially increasing the surface reflectance.

tops of the buildings), and then 2-m temperatures were calculated for each surface. No surface evaporation from the impervious surfaces was allowed (which is a reasonable assumption in the absence of rainfall or assuming complete runoff).

b. *Effective surface temperature*

The comfort of a person is probably more closely related to his/her radiative and thermal energy balance than on ambient air temperature alone. Monteith (1971) defines an effective air temperature T_e that accounts for the radiative and sensible heat balance on a body. By simplifying Monteith's formulation by eliminating evaporation and metabolic heat generation from the body, the effective temperature can be written as

$$T_e = T_a + R_a R_{\mathrm{nb}}, \tag{1}$$

where T_a is the air temperature near the person, R_{nb} is the net radiation absorbed by the body, and R_a is the atmospheric resistance of heat flow from the body to the air, and depends upon the wind speed (as noted below). In addition to metabolic heat generation or evaporation, ambient humidity is also not included, because it would affect only a wet system in which evaporation is taken into account. Note that the equation implicitly includes the sensible heat loss from the body.

A simple radiative balance for a spherical body exposed to an external environment is expressed in Fig. 3. The sphere is meant to crudely represent a bare, unclothed head. The depiction is obviously highly artificial, but it nevertheless captures the essential (though perhaps not all) factors that figure in the comfort of an individual exposed to the surroundings. The net radiation for a person R_{nb} is the sum of individual radiative components such as direct and indirect shortwave radiation, the first three terms on the right-hand side of Eq. (2) below, which express the solar balance on the body. The remaining three terms on the right-hand side express longwave radiation emitted from above and below and longwave fluxes emitted from a person:

$$R_{\mathrm{nb}} = S_d(1-\alpha_b) \times \mathrm{SF} + S_{\mathrm{df}}(1-\alpha_b) + 0.5(S_d)\alpha_g(1-\alpha_b) + 0.5L_d + 0.5L_g - L_b, \tag{2}$$

where S_d is the direct shortwave radiation incident on a person, α_b is the albedo of a person's skin, SF is a shape factor for direct solar radiation incident on a body (0.25 for a sphere), S_{df} is the diffuse shortwave radiation, α_g is the ground surface albedo, L_d is the downward longwave (thermal) radiation from the atmosphere, L_g is the blackbody radiation emitted from the ground and absorbed by the lower half of the sphere, and L_b is the

blackbody radiation emitted from the body. Based on Monteith (1971), the atmospheric resistance R_a between skin and air, which governs the sensible heat loss from the body, was set as

$$R_a = (12V^{1/2})^{-1}, \quad (3)$$

where V (m s^{-1}) is the ambient wind speed at 2 m [but R_a has units of K (W m^{-2})$^{-1}$].

Further assumptions made to calculate T_e from the MM5 SEBM model output are that 1) the absorption of radiant energy on the body is expressed in terms of absorption by bare skin of the head, 2) the head is a round object and the effects of hat and hair on the head temperature are ignored, 3) the surface emissivity of all solid objects is equal to 1.0, 4) the albedo of the skin $\alpha_b = 0.2$, and 5) the shape factor for direct solar flux of a round object SF = 0.25. The factors of 0.5 in front of the reflection of radiation from the ground surface and thermal radiation terms pertain to the fact that these components are incident on just the top half or just the bottom half of the head. 6) The direct radiation was assumed to be 0.9 of the total incident shortwave radiation at the surface. Thus, the total heat stress on the body is effectively determined by the net radiation balance on the body while accounting for sensible heat loss. Note that the ground surface heat flux does not figure in the perception of comfort, although it is important in affecting the other parameters in Eq. (2).

Because we did not have 2-m winds from the model output, we used the wind speeds at 10 m, causing a slight underestimate of the stress on a person. Further, the LSM does not calculate radiometric temperatures for the ground and leaf surface or air temperatures under vegetation cover. Instead, to calculate the energy balance of the person under a tree, we assume that the air temperature and ground temperatures under the tree are equal to the 2-m air temperatures for the tree surfaces and that no direct solar flux is incident on or reflected to the person. For the grass and impervious surfaces, both the surface skin temperature and 2-m temperatures are used, and solar flux is both incident and reflected on the person. Last, we assume that the person's skin temperature is 35°C for calculating the longwave flux from the body.

This formulation for comfort contains elements of other comfort indices, such as the windchill temperature (Steadman 1971), but here it is specific to a hypothetical bare head of a person standing over pavement, under a tree or on a grass surface in an urban environment.

c. Simulation experiments

It would have been preferable to specify land surface parameters based on actual measurements or as a function of sun angle (in the case of albedo). However, circumstances were such that albedo, vegetation fraction, and initial soil moisture were specified as a function of surface type (which themselves vary spatially within the domain), which is actually the standard procedure in MM5. Within the city, very high resolution data were used to specify the percentage of each surface within each grid element of MM5.

To obtain high-resolution simulation results, MM5 was first simulated using National Centers for Environmental Prediction (NCEP) reanalysis data to force a double nest (12 and 4 km) within a 36-km coarse domain (not shown). The starting date was 10 August, and the simulation continued until 16 August (154 h; the data were output every hour). The vertical grid in the model was a stretched vertical coordinate, with the highest resolution of a few tens of meters in the surface layer. The Eta boundary layer scheme was used with the Rapid Radiative Transfer Model radiation package. The Kain–Fritsch cumulus parameterization was used on the outer grids but not on the 4- or 1.3-km grids, for which only the "Reisner2" bulk parameterization was used. Five simulations were produced using the 4-km output as initial and lateral boundary conditions for a 1.3-km high-resolution domain. The first used LSUM to simulate 150 h of meteorological conditions on a 1.33-km grid. The remaining four experiments were done using SEBM with the observed set of initial conditions (one experiment) and SEBM with three mitigation scenarios (although these last three simulations proceeded only for 126 h). The model simulations began 10 August 2001. No significant rain amounts were recorded in NYC during the simulation period.

The three mitigation scenarios are 1) planting trees on streets, 2) planting trees on grassy areas, and 3) raising the albedo of the impervious surface from 0.15 to 0.5. Figure 4 shows the percentages of street area that can be converted to trees; the percentage of grassy areas that can be converted to trees is the same as the percentage of existing grassy areas.

d. Observational data

The surface air data for this study were obtained from National Weather Service observing stations [John F. Kennedy International Airport (JFK), Central Park, and La Guardia Airport (LGA)] and from WeatherBug stations situated throughout NYC on rooftops and other locations. Figure 5 shows the location of the observing stations used here. In this study, observed surface 2-m temperatures, relative humidity (RH), and surface wind speeds are compared with model results. For the weather station sites, the winds were observed at 10-m heights.

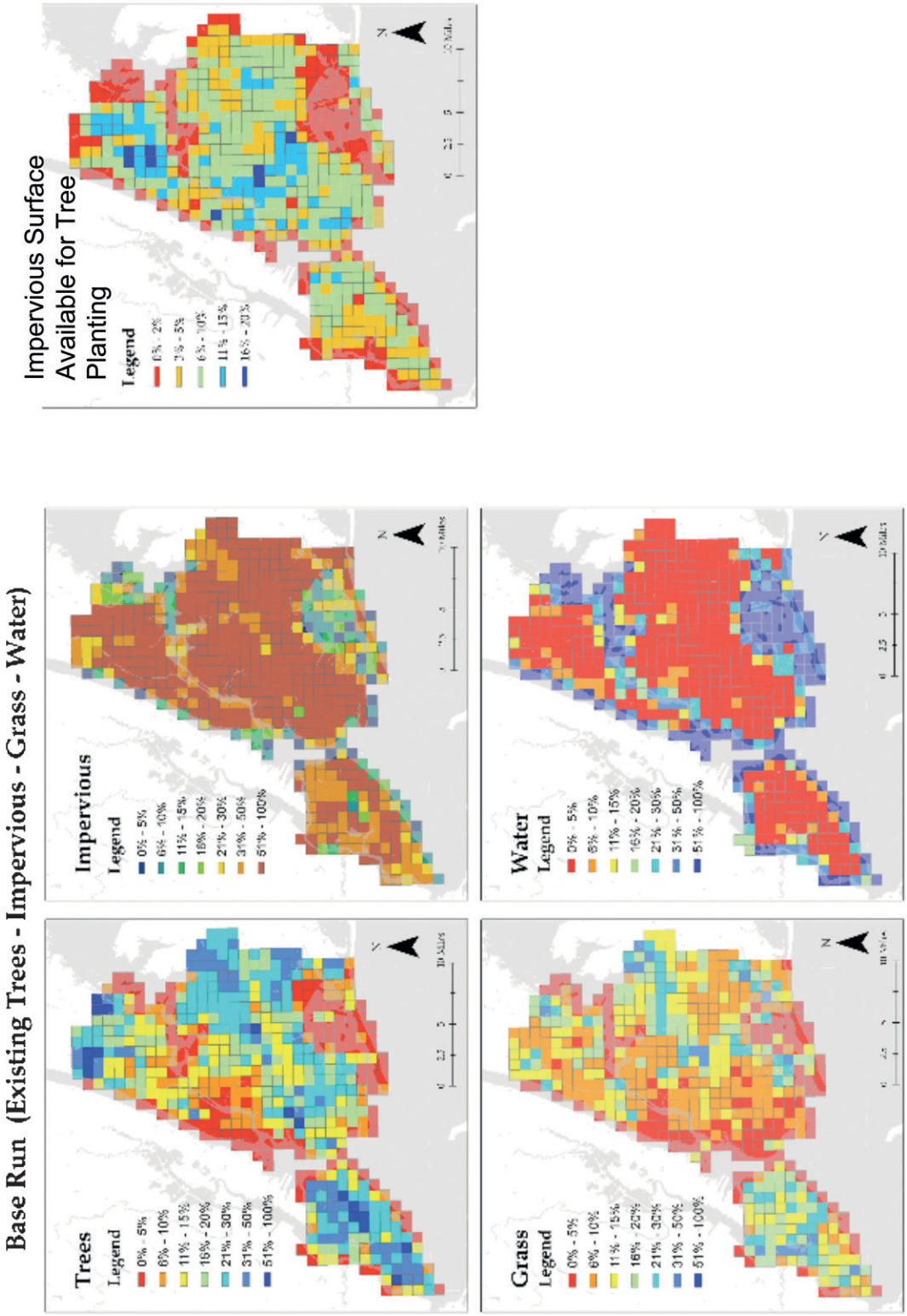

FIG. 4. The percentage of each surface within the NYC five-county area. Also shown are the percentages of impervious surfaces that could be converted to tree coverage. The percentage of grassy surface that can be converted to tree coverage was assumed to be equal to the percentage of grassy surfaces.

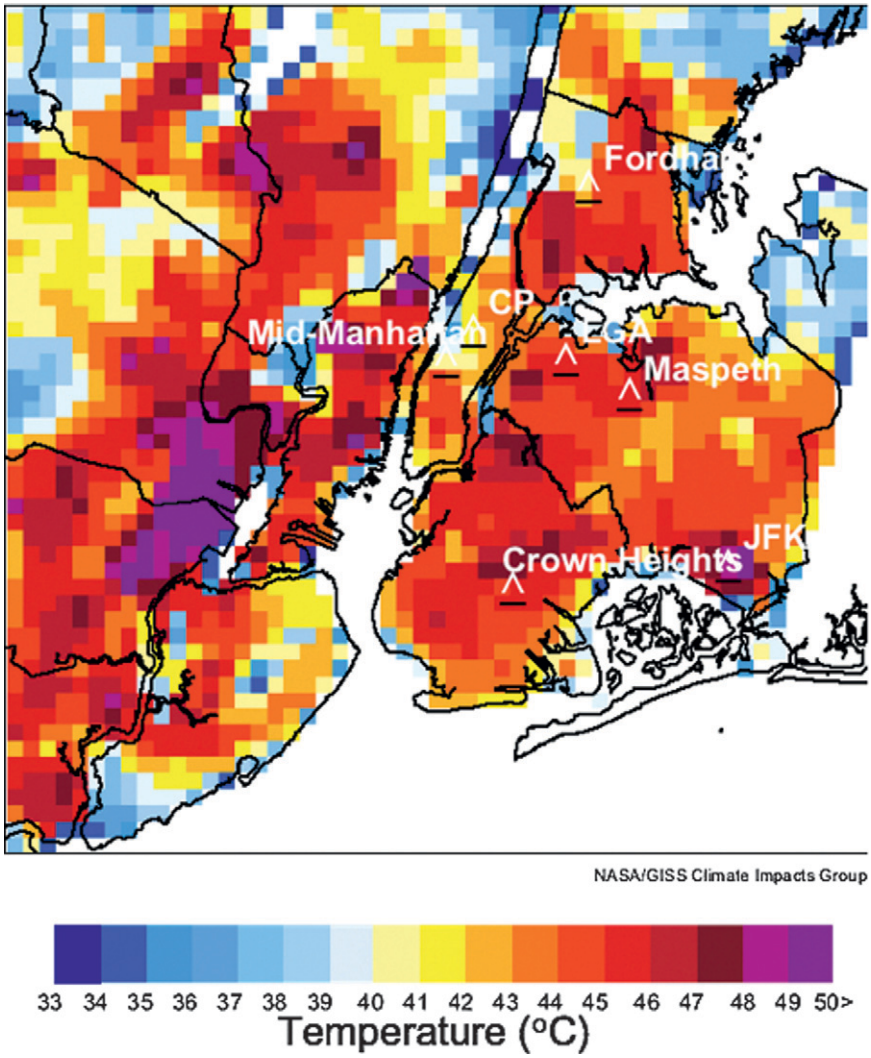

FIG. 5. The 1-km satellite-calculated skin temperature of the NYC (and Newark) metropolitan areas for 1030 LST 14 Aug 2002. The data from the labeled surface stations were used in the study to verify the model simulations.

The surface temperatures were used "as is." The surface humidity and wind speeds were filtered using a third-order polynomial (with coefficients 1:4:6:4:1). This was done to reduce the high-frequency variability in these variables and to obtain a more meaningful comparison with model results. The model data were interpolated to the location of the observational data using a linear interpolation of the four surrounding points.

A comparison is also made between surface radiometric temperatures from the *Landsat 7* Thematic Mapper imagery band 6L/H and MM5's surface (ground) radiometric temperatures. The Landsat data were at 60-m resolution. The digital number (DN) thermal band 6L (low gain) was converted to radiance and then to the surface radiometric temperature using standard algorithms developed by the Landsat Science Team. The results of this multistep process are presented in Fig. 5, which shows the radiometric surface ("skin") temperatures at 1030 LST 14 August 2001, covering an area larger than the area of the mitigation study shown in Fig. 4. One notes that the radiometric surface temperatures vary substantially over areas both within the mitigation domain and without as the result of the spatial variation in surface characteristics.

The mean radiometric surface temperature within the mitigation area (see Fig. 4) was higher than that obtained from MM5 (see below). No effort was made to reconcile this discrepancy, although such a discrepancy is not surprising in view of the imperfect correction of the raw satellite temperatures for atmospheric attenuation due to the presence of water vapor and carbon dioxide. Alternatively, the surface roughness length for heat

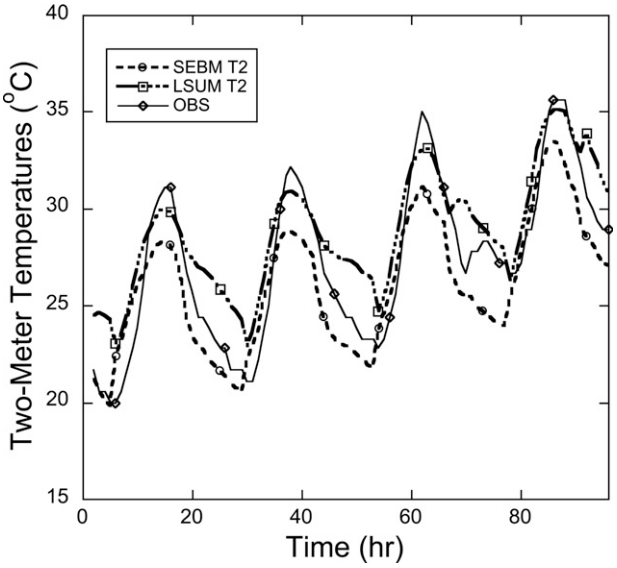

FIG. 6. Simulated 2-m temperature for Central Park obtained on days 1–4 using MM5 with either LSUM or SEBM. The simulated days correspond to 10–14 Aug 2001. The grid size was 1.3 km.

used in the model might have been too large, although surface temperatures simulated with SEBM, which depend on the simulated ground/radiometric temperatures, were very good, as shown below.

3. Results

a. Model verification

Figure 6 shows the simulated model temperatures from LSUM and SEBM from the first four days of model simulation, beginning on 10 August, from Central Park. On the first three days, both LSUM and SEBM exhibit a strong negative bias in the maximum temperature, although the bias in SEBM is larger than in LSUM. Later, near the end of the four-day period (after 72 h; 13 August), however, the low bias in both models is smaller, suggesting that both simulations required ''spinup'' time to better equilibrate the model initial soil moisture with the atmospheric forcing. As an alternative, smaller values of soil moisture might have been chosen to better ''fit'' the data earlier in the simulations.

Figures 7, 8, and 9, respectively, show the observed temperature, relative humidity, and 10-m winds from Central Park for 13–15 August obtained using SEBM and LSUM within MM5. Although both models roughly capture the timing and amplitudes of maxima and minima, SEBM seems to perform somewhat better, at least with regard to the 2-m temperatures in Central Park.

Tables 2 and 3 show the bias and root-mean-square error from Central Park and six other observing stations in the NYC five-county area, calculated for the time period after the land surface model results indicate closer equilibrium between the soil conditions and the atmosphere. For this time period, from 0700 LST 13 to 0600 LST 16 August, SEBM simulated more realistic surface temperatures and wind speeds at most of the observing stations. SEBM also simulated smaller average absolute bias and root-mean-square error than did LSUM. SEBM, however, simulated a larger bias in the humidity than did LSUM. When only the National Weather Service

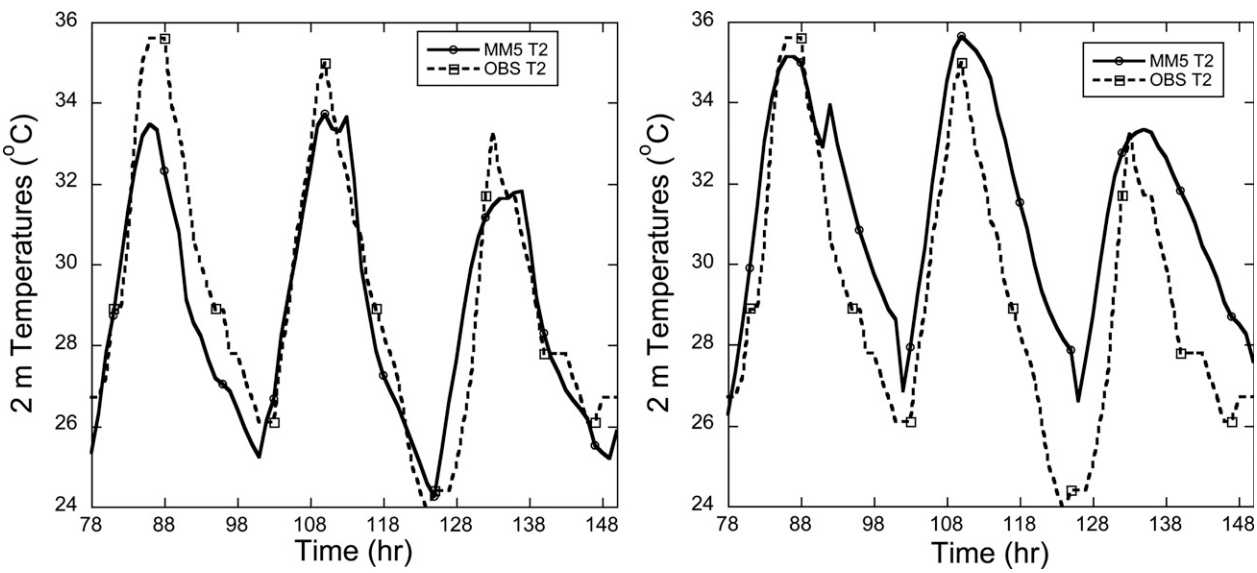

FIG. 7. As in Fig. 6, but for 0600 LST 13 Aug–0600 LST 16 Aug for (left) SEBM and (right) LSUM.

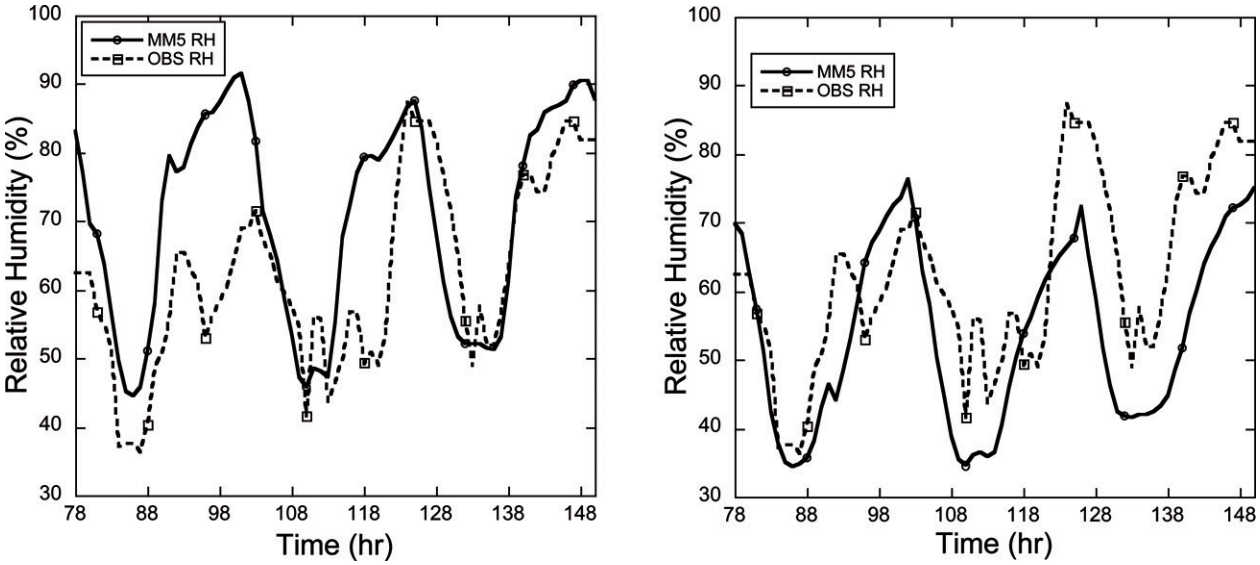

FIG. 8. As in Fig. 7, but for the (time filtered) RH.

stations are compared, SEBM simulated better temperature and humidity statistics.

As noted, SEBM had a larger cool bias on 13 August than did LSUM. However, the mean soil water content in an MM5 (SEBM) grid element is determined from a mix of impervious and pervious surfaces, whereas such surfaces in LSUM would likely be classified as ''urban/impervious,'' thus possibly accounting for SEBM's longer time to spin up. When the data from 0700 LST 13 through 0600 LST 16 August are excluded, SEBM also simulated smaller bias in the humidity than did LSUM (cf. Tables 2 and 3), as well as smaller temperature and wind biases.

For comparison with the satellite radiometric temperatures, simulated surface ground temperatures at 1000 and 1100 LST 14 August 2001 were averaged to obtain values at 1030 LST, the approximate time of satellite overpass. We noted that there was a discrepancy between the model simulated radiometric (ground) temperatures and those obtained using satellite retrievals, which was about 4°C. Instead of a single plot for each model and the satellite temperatures, we plotted all of the data on a single axis (Fig. 10) by subtracting 4°C from the satellite temperatures. In this case, it becomes apparent that the LSUM distribution is shifted notably to the warm side of the observations relative to the observed and simulated distributions of

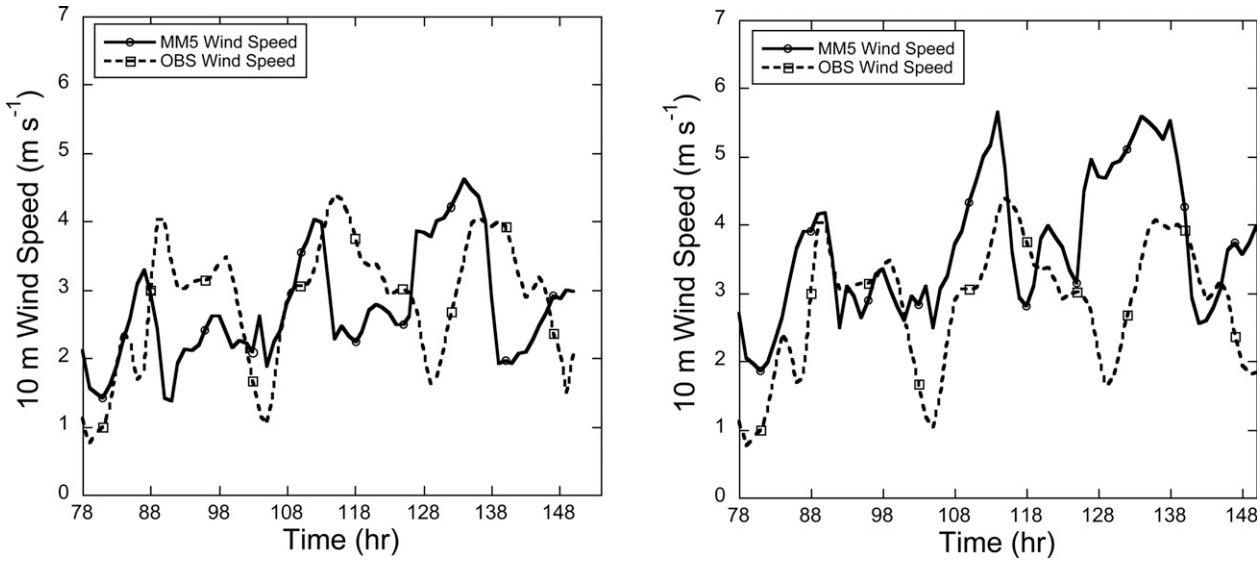

FIG. 9. As in Fig. 7, but for the (time filtered) surface 10-m wind speed.

TABLE 2. Model statistics that compare SEBM results with observations. The mean and bias include the data from 0700 LST 13 Aug to 0600 LST 16 Aug 2001. The mean of the sum of the absolute values over the seven individual stations is given for two time periods, as indicated in the last two rows.

Station	Bias T (°C)	RMSE T (°C)	Bias wind speed (m s^{-1})	RMSE wind speed (m s^{-1})	Bias RH (%)	RMSE RH (%)
JFK	1.51	2.00	−1.98	2.92	−0.82	7.15
LGA	2.14	2.67	−2.17	2.73	−0.25	13.88
Central Park	−0.39	1.32	−0.09	1.35	8.24	14.35
Crown Heights	1.25	2.05	2.76	2.87	6.36	13.90
Mid-Manhattan	−1.20	2.39	0.04	1.39	22.11	27.74
Maspeth	1.06	1.95	0.36	1.39	8.88	14.96
Fordham	−0.71	1.56	1.49	1.64	9.23	14.88
Absolute mean (0700 LST 13–0600 LST 16 Aug)	1.18	1.99	1.27	2.04	7.99	15.27
Absolute mean (0700 LST 14–0600 LST 16 Aug)	1.32	1.98	1.34	2.13	5.70	12.03

SEBM, most likely because it does not explicitly reproduce contributions from nonimpervious surfaces within the simulated urban-defined grid element.

b. Mitigation strategies

Figures 11, 12, and 13 show, respectively, examples of mitigation strategy impacts on surface air temperatures at 1200 and 1800 LST 14 August 2001 and at 0000 LST 15 August 2001. Also shown are the temperatures from the base SEBM run (labeled "control") for reference. At 1200 LST, increasing the albedo of the impervious surfaces had a much larger cooling impact on 2-m temperatures than did planting trees on impervious surfaces or on grass. The largest effects of the various mitigation strategies were obtained at 1800 LST (Fig. 12). At this time, both strategies were effective at reducing surface air temperature. In both cases, the strongest decrease in surface 2-m temperatures was obtained in the city urban core. The impact of each strategy on surface temperatures was readily apparent even at 0000 LST (Fig. 13) of the next day, before mostly dissipating by morning (not shown).

Figure 14 shows the effective aggregate surface temperatures obtained from the SEBM control at 1200 LST 14 August 2001, as compared with individual impervious, grass, and tree surfaces. Note that the effective temperatures from the impervious, grass, and tree surfaces (and water) were used in their observed percentages (Fig. 4) to calculate the aggregate effective temperatures of the SEBM control. To reiterate, these figures give a quantitative temperature that reflects the comfort of a person standing on the impervious or grass surfaces or under a tree relative to the average or aggregate temperature within each grid element (note that the calculation is relevant to a person's bare head). The effective surface temperature over the impervious surface is larger than the aggregate, and the effective surface temperature under the trees is much less than the aggregate. Many locations on the grassy surfaces also exhibit positive differences in effective temperature, although fewer than on the impervious surface.

The effective surface temperatures for the impervious surfaces in Fig. 14 were obtained with an albedo of 0.15 for this surface. Figure 15 shows the aggregate effective temperature from a simulation with the albedo of the impervious surface set equal to 0.5. Also shown is the difference in effective temperature between the impervious surface with an albedo of 0.5 and the aggregate surface. Although the aggregate surface effective temperatures in Figs. 15 and 14 are very similar, an

TABLE 3. As in Table 2, but for LSUM.

Station	Bias T (°C)	RMSE T (°C)	Bias wind speed (m s^{-1})	RMSE wind speed (m s^{-1})	Bias RH (%)	RMSE RH (%)
JFK	0.93	1.50	−0.89	2.55	0.24	8.02
LGA	3.61	3.82	−1.29	2.12	−12.31	17.64
Central Park	2.08	2.43	0.87	1.55	−8.11	13.13
Crown Heights	2.32	2.73	3.43	3.60	−1.69	12.16
Mid-Manhattan	1.39	1.93	1.35	1.98	3.62	12.35
Maspeth	2.44	2.82	1.11	1.74	−0.43	11.62
Fordham	1.43	2.07	2.24	−0.75	11.00	—
Absolute mean (0600 LST 13–0600 LST 16 Aug)	1.93	2.38	1.57	2.25	3.88	12.28
Absolute mean (0700 LST 14–0600 LST 16 Aug)	2.41	2.67	1.70	2.44	6.93	12.22

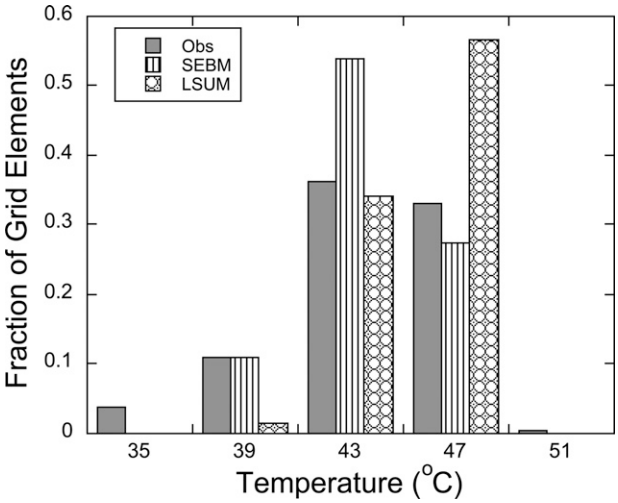

FIG. 10. Histogram of observed and simulated radiometric surface temperature at 1030 LST 14 Aug 2001. The data from the observed radiometric satellite temperatures have been translated (moved to the left, or toward lower temperature) by 4°C along the x axis.

increase in albedo from 0.15 to 0.5 would greatly affect the comfort of a person standing over an impervious surface at noon (1200 LST), which suggests that a person would generally feel between 3° and 6°C warmer than when standing on a surface with albedo of 0.15, even if the actual air temperature was reduced by the increase in surface albedo, as shown in Figs. 11–13.

Figure 16 shows two components of the energy balance for the model person used to calculate effective surface temperatures: the reflected shortwave energy from the ground surface and the longwave radiation emitted by this surface for each hour on 14 August 2001 (the downwelling components remained nearly unchanged and are not shown). The model data were averaged over the mitigation area. Grassy and impervious surfaces with an albedo of 0.15 have similar amounts of shortwave radiation reflected by the ground and absorbed by the person, whereas there is very little reflected radiation on a person standing under a tree. In contrast, the (relatively hot) impervious surfaces emit much more longwave radiation than do the grass and

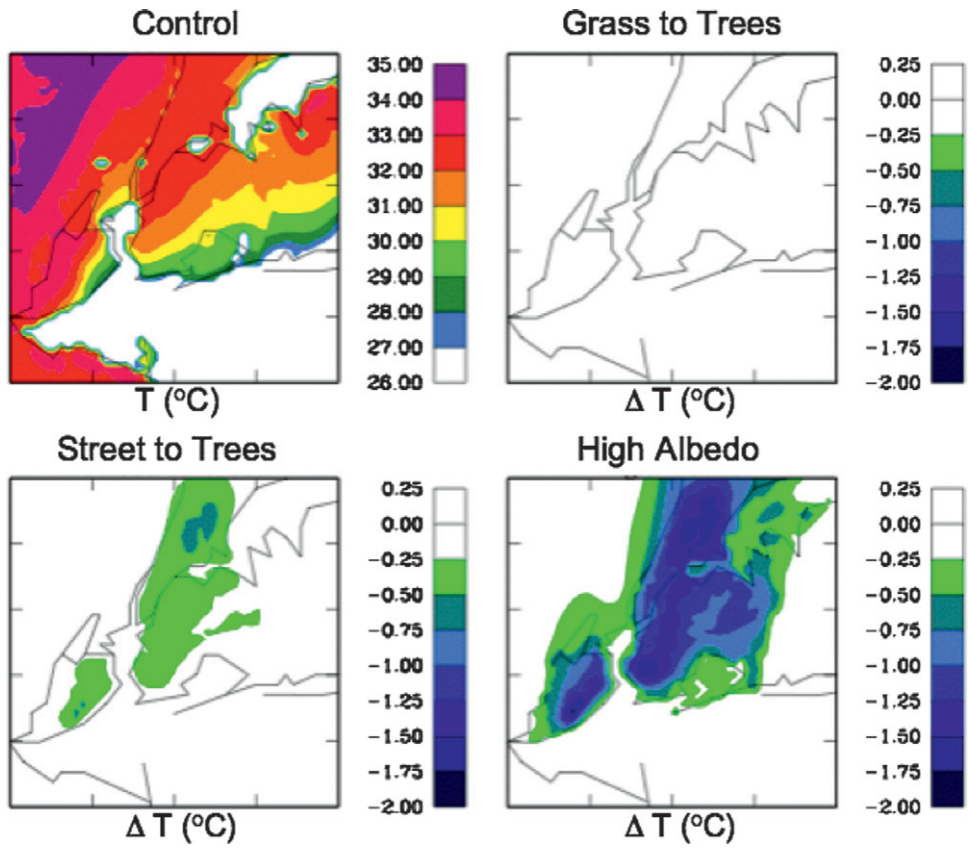

FIG. 11. Simulated impacts of three mitigation strategies on the (top left) surface 2-m temperature T (°C) at 1200 LST 14 Aug 2001. These strategies are (top right) converting grass to trees, (bottom left) converting streets to trees, and (bottom right) changing the albedo of the impervious surfaces from 0.15 to 0.50.

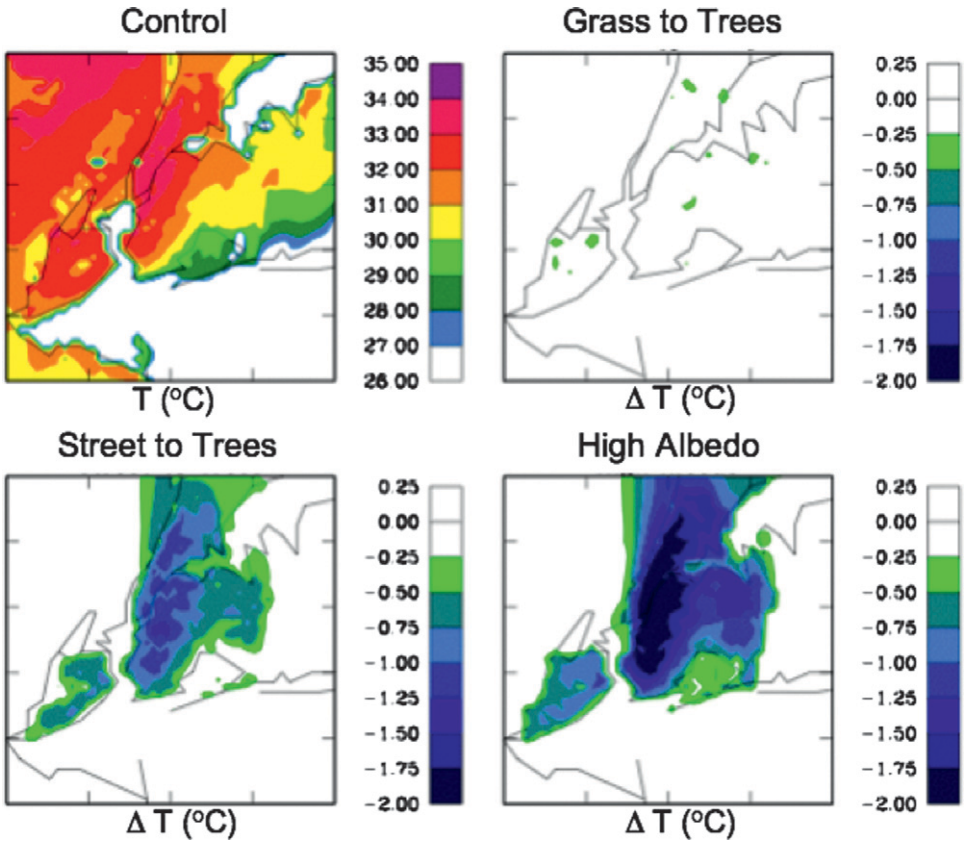

FIG. 12. As in Fig. 11, but for 1800 LST.

especially the tree surfaces (which are relatively cooler). When the surface albedo of the impervious surface was increased to 0.5, leading to a relative cooling of this surface, the impervious surface emitted less radiation than before (and even a little less than the grassy surface). However, the peak amount of shortwave radiation reflected on the person more than tripled in magnitude. Hence, increasing the surface albedo of the impervious surfaces led to a net gain on the person (at 1200 LST) of nearly 80 W m^{-2}. (Skiers will have no trouble understanding the effect of snow cover in increasing the amount of solar radiation incident on their body.)

The effective temperature and the air temperature (not shown) were very similar at 1800 LST for a person standing under a tree or on the high albedo surface (or even grass). Not surprising, therefore, is that the effective temperature as a measure of human comfort has the greatest impact during periods of high sun.

4. Discussion and conclusions

A new surface layer formulation that allows multiple roughness regimes to apply at a single grid point within a mesoscale model was developed to identify efficient strategies for mitigating increases in surface air temperatures associated with the urban heat island in the New York City five-county area. The new surface formulation, though lacking a surface urban canyon component, allows the user flexibility in specifying multiple ground cover types at one grid point. Results were satisfactory and constituted an improvement over the conventional surface layer formulation once the model was allowed to equilibrate. This formation also led to improved simulation of wind speeds relative to the MM5 LSUM. The most likely reason for this is the use of the global roughness length for the cityscape versus the local roughness lengths for the underlying city surfaces.

Perhaps the most pertinent result is that increasing the albedo of the street, while serving as an effective means for reducing surface air temperatures, increased the noontime thermal stress on a hypothetical individual at street level as the result of reflected solar radiation and emitted thermal radiation from below. Although less effective in reducing the air temperature, trees provided the best combination of reducing late afternoon/evening surface temperature and noontime radiation stress on a person at sidewalk level.

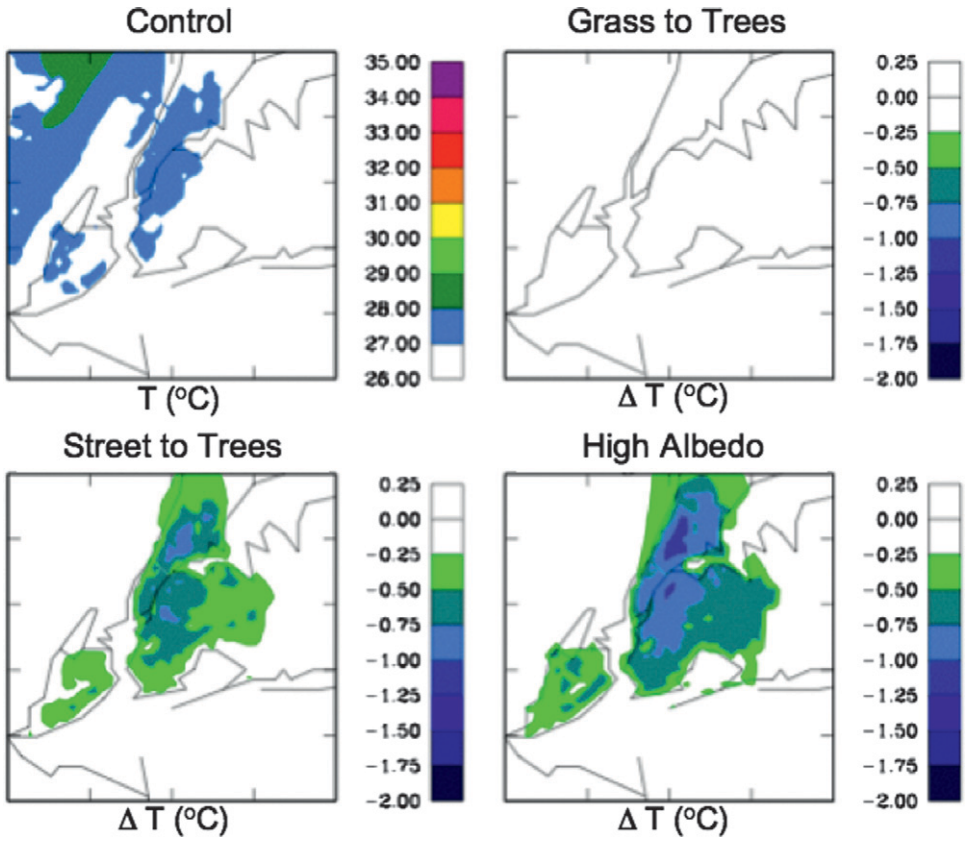

FIG. 13. As in Fig. 11, but for 0000 LST 15 Aug 2001.

This result demonstrates that the comfort of a person, as measured by the effective temperature on a person standing at street level, does not depend solely on air temperature but also on the heat and radiation balance on that person. A person standing under a tree has a much lower effective temperature than a person on the street during the time of high incident solar radiation (e.g., 1200 LST). Increasing the surface albedo therefore is an ineffective, if not detrimental, method for improving the comfort of pedestrians in a city such as New York. The reason is that the hot, paved surface both emits and reflects solar and thermal radiation back to the individual. Increasing albedo does reduce the amount of absorbed solar flux at the surface and thereby reduces the surface temperature and the emitted thermal flux, but the increase of reflected solar flux from the ground more than offsets the decrease in thermal radiation emitted upward from the ground.

The presence of shade trees, however, reduces the energy load on a person by blocking downward solar radiation and thereby reducing the amount of reflected shortwave radiation from the surface. Upward thermal radiation from the surface is also reduced in this case because the surface under the tree is also cooler than in direct sunlight. Planting trees on grassy surfaces had relatively little effect on the surface 2-m temperature. The impact of planting trees on grassy surfaces would probably have been higher if the initial soil moisture of the first layer of the soil was assumed to be closer to wilting than to saturation.

This discussion calls into question what is commonly referred to as the urban heat island effect. The UHI, as noted, is a measure of air temperature and is usually a maximum at night, in response to the release of stored heat from city surfaces. However, the calculation of effective surface temperature indicates that the urban heat island's impact on the city inhabitants during high noon is actually as large as or larger than the nocturnal heat island. Planting trees reduces this particular (previously undocumented) aspect of the UHI, as well as elevated temperatures that would occur at the city surface after sundown.

Our scheme can also be modified to simulate rooftops and streets/canyons separately, given the relative percentages of each. As in Chin et al. (2005), this would allow us to account explicitly for radiation differences between street level and roof top. The approached outline here could also be applied to the newest version of

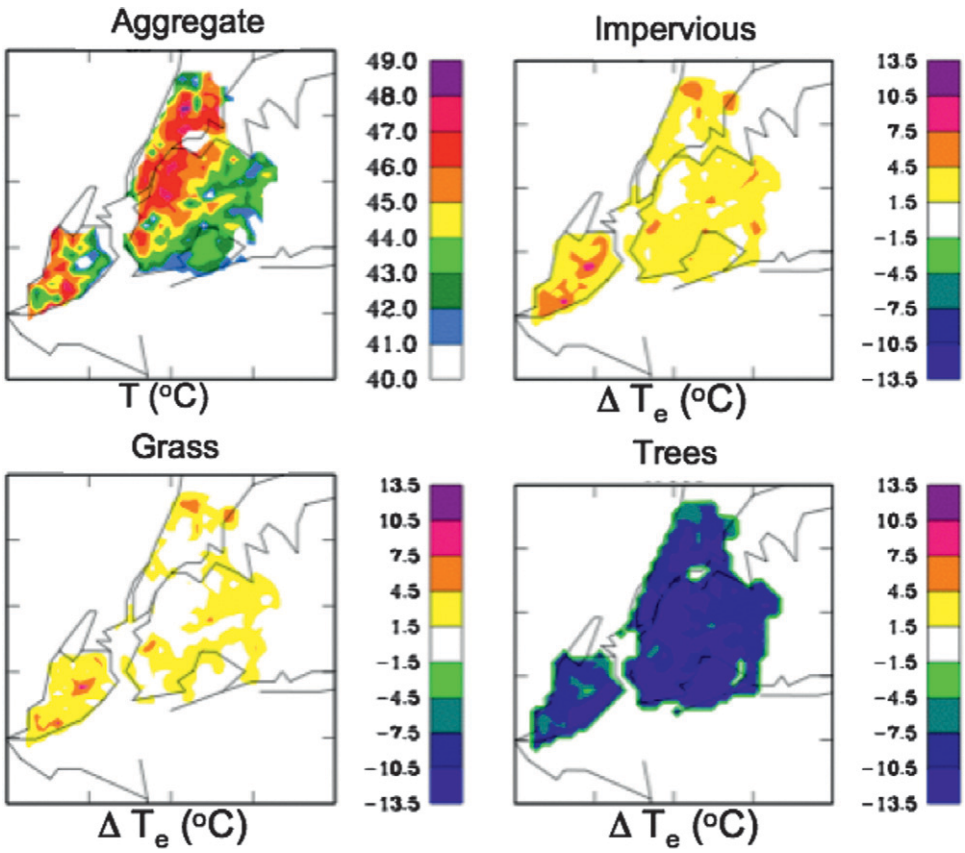

FIG. 14. (top left) The spatial distribution of the (aggregate) effective temperature T_e (°C) obtained in the control experiment with SEBM at 1200 LST 14 Aug 2001. The spatial distribution of differences between the aggregate temperature and the effective temperature of a person standing (top right) above an impervious surface, (bottom left) above grass, or (bottom right) under a tree.

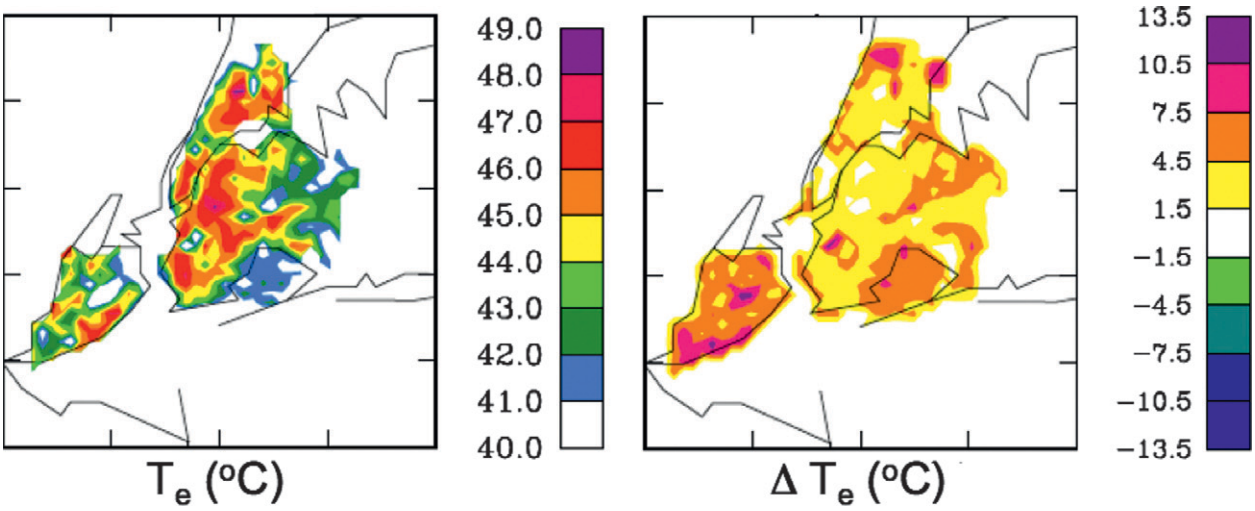

FIG. 15. (left) The spatial distribution of aggregate effective temperature for a simulation with an albedo for the impervious surface of 0.5, and (right) the spatial distribution of the difference between the aggregate and the effective surface temperatures of a person standing on an impervious surface with an albedo of 0.5.

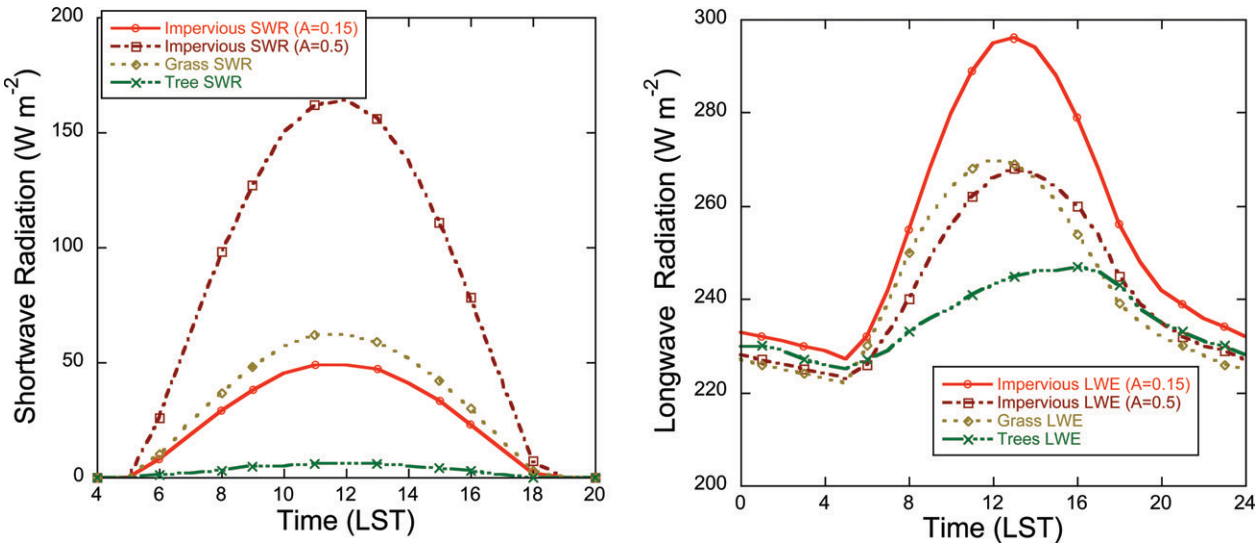

FIG. 16. Shortwave and longwave components of the effective temperature energy balance for 14 Aug 2001 for a person standing on the different surfaces shown. The shortwave energy is reflected from the surface and is absorbed on the person; the longwave energy is emitted from the surface and is absorbed on the person.

the WRF urban canopy model. This model is also based on the Noah LSM but includes a detailed urban canopy model of Kusaka et al. (2005). We suppose that the implementation of newer, more sophisticated urban canopy models in the WRF, combined with our method of assigning more than one roughness length to each grid element, should allow for even higher accuracy in the calculation of surface temperatures and so on.

Acknowledgments. This project was funded by NYSERDA as part of two New York Energy $mart programs: the Peak Load Reduction Program (PRLP) and the Environmental Monitoring, Evaluation, and Protection (EMEP) Program. Funding support was also provided by the U.S. Department of Agriculture Forest Service in collaboration with the New York State Department of Environmental Conservation (DEC). The views expressed do not necessarily reflect those of the New York State Department of Environmental Conservation.

REFERENCES

Ackerman, B., 1985: Temporal march of the Chicago heat island. *J. Climate Appl. Meteor.,* **24,** 547–554.

Arnfield, J. A., 2003: Two decades of urban climate research: A review of turbulence, exchanges of energy and water, and the urban heat island. *Int. J. Climatol.,* **23,** 1–26.

Balling, R. C., and R. S. Cerveny, 1987: Long-term associations between wind speeds and the urban heat island of Phoenix, Arizona. *J. Climate Appl. Meteor.,* **26,** 712–716.

Bornstein, B., 1968: Observations of the urban heat island effect in New York City. *J. Appl. Meteor.,* **7,** 575–582.

Chen, F., and J. Dudhia, 2001a: Coupling an advanced land surface–hydrology model with the Penn State–NCAR MM5 modeling system. Part I: Model implementation and sensitivity. *Mon. Wea. Rev.,* **129,** 569–585.

——, and ——, 2001b: Coupling an advanced land surface–hydrology model with the Penn State–NCAR MM5 modeling system. Part II: Preliminary model validation. *Mon. Wea. Rev.,* **129,** 587–604.

——, D. N. Yates, H. Nagai, M. A. LeMone, K. Ikeda, and R. L. Grossman, 2003: Land surface heterogeneity in the Cooperative Atmosphere Surface Exchange Study (CASES-97). Part I: Comparing modeled surface flux maps with surface flux tower and aircraft measurements. *J. Hydrometeor.,* **4,** 196–218.

Chin, H.-N. S., M. M. Leach, G. A. Sugiyama, J. M. Leone Jr., H. Walker, and J. S. Nasstrom, 2005: Evaluation of an urban canopy parameterization in a mesoscale model using VTMX and URBAN 2000 data. *Mon. Wea. Rev.,* **133,** 2043–2068.

Civerolo, K. L., G. Sistla, S. T. Rao, and D. J. Nowak, 2000: The effects of land use in meteorological modeling: Implications for assessment of future air quality scenarios. *Atmos. Environ.,* **34,** 1615–1621.

Coutts, A. M., J. Beringer, and N. J. Tapper, 2007: Impact of increasing urban density on local climate: Spatial and temporal variations in the surface energy balance in Melbourne, Australia. *J. Appl. Meteor. Climatol.,* **46,** 477–493.

Dudhia, J., 1993: A nonhydrostatic version of the Penn State–NCAR mesoscale model: Validation tests and simulation of an Atlantic cyclone and cold front. *Mon. Wea. Rev.,* **121,** 1493–1513.

Dupont, S., T. Otte, and J. Ching, 2004: Simulation of meteorological fields within and above urban and rural canopies with a mesoscale model. *Bound.-Layer Meteor.,* **111,** 111–158.

Gallo, K. P., A. L. McNab, T. R. Karl, J. F. Brown, J. J. Hood, and J. D. Tarpley, 1993: The use of NOAA AVHRR data for assessment of the urban heat island effect. *J. Appl. Meteor.,* **32,** 899–908.

Grell, G. A., J. Dudhia, and D. R. Stauffer, 1994: A description of the fifth-generation Penn State/NCAR mesoscale model (MM5). NCAR Tech. Note NCAR/TN-398+STR, 121 pp.

Grossman-Clarke, S., J. A. Zehnder, W. L. Stefanov, Y. Liu, and M. A. Zoldak, 2005: Urban modifications in a mesoscale meteorological model and the effects on near-surface variables in an arid metropolitan region. *J. Appl. Meteor.,* **44,** 1281–1297.

Hawkins, T. W., A. J. Brazel, W. L. Stefanov, W. Bigler, and E. M. Saffell, 2004: The role of rural variability in urban heat island determination for Phoenix, Arizona. *J. Appl. Meteor.,* **43,** 476–486.

Holt, T., and J. Pullen, 2007: Urban canopy modeling of the New York City metropolitan area: A comparison and validation of single- and multilayer parameterizations. *Mon. Wea. Rev.,* **135,** 1906–1930.

Huang, Y. J., H. Akbari, H. Taha, and A. H. Rosenfeld, 1987: The potential of vegetation in reducing summer cooling loads in residential buildings. *J. Appl. Meteor.,* **26,** 1103–1116.

Kim, Y.-H., and J.-J. Baik, 2002: Maximum urban heat island intensity in Seoul. *J. Appl. Meteor.,* **41,** 651–659.

Kunkel, K. E., S. A. Changnon, and B. C. Reinke, 1996: The July 1995 heat wave in the Midwest: A climatic perspective and critical weather factors. *Bull. Amer. Meteor. Soc.,* **77,** 1507–1518.

Kusaka, H., and F. Kimura, 2004: Thermal effects of urban canyon structure on the nocturnal heat island: Numerical experiments using a mesoscale model coupled with an urban canopy model. *J. Appl. Meteor.,* **43,** 1899–1910.

——, F. Chen, T. Muku, and H. Hiromaru, 2005: Impact of the urban canopy model in the next-generation numerical weather prediction model, WRF. *Environ. Syst. Res.,* **33,** 159–164.

Liu, Y., F. Chen, T. Warner, and J. Basara, 2006: Verification of a mesoscale data assimilation and forecasting system for the Oklahoma City area during the Joint Urban 2003 Field Project. *J. Appl. Meteor.,* **45,** 912–929.

Livezey, R. E., and R. Tinker, 1996: Some meteorological, climatological, and microclimatological considerations of the severe U.S. heat wave of mid-July 1995. *Bull. Amer. Meteor. Soc.,* **77,** 2043–2054.

Monteith, J. L., 1971: *Principles of Environmental Physics*. Arnold, 241 pp.

Myrup, L. O., 1969: A numerical model of the urban heat island. *J. Appl. Meteor.,* **8,** 908–918.

Nowak, D., K. Civerolo, S. T. Rao, G. Sistla, C. Luley, and D. Crane, 2000: A modeling study of the impact of urban trees on ozone. *Atmos. Environ.,* **34,** 1601–1613.

Ohashi, Y., and H. Kida, 2002: Local circulations developed in the vicinity of both coastal and inland urban areas: A numerical study with a mesoscale atmospheric model. *J. Appl. Meteor.,* **41,** 30–45.

Oke, T. R., 1976: The distinction between canopy and boundary layer urban heat islands. *Atmosphere,* **14,** 268–277.

Otte, T. L., A. Lacser, S. Dupont, and J. K. S. Ching, 2004: Implementation of an urban canopy parameterization in mesoscale meteorological model. *J. Appl. Meteor.,* **43,** 1648–1665.

Pielke, R., 1984: *Mesocale Meteorological Modeling*. Academic Press, 612 pp.

Roberts, S. M., T. R. Oke, C. S. B. Grimmond, and J. A. Voogt, 2006: Comparison of four methods to estimate urban heat storage. *J. Appl. Meteor. Climatol.,* **45,** 1766–1781.

Sailor, D. J., and H. Fan, 2004: The importance of including anthropogenic heating in mesoscale modeling of the urban heat island. Preprints, *Symp. on Planning, Nowcasting, and Forecasting in the Urban Zone,* Seattle, WA, Amer. Meteor. Soc., 3.5. [Available online at http://ams.confex.com/ams/pdfpapers/74444.pdf.]

Seguin, B., and N. Gignoux, 1974: Etude expérimentale de l'influence d'un réseau de brise-vent sur le profil vertical de vitesse du vent [Experimental study of the influence of a network of wind barriers (hedgerows) on the vertical profile of wind speed]. *Agric. For. Meteor.,* **13,** 15–23.

Steadman, R. G., 1971: Indices of wind chill of clothed persons. *J. Appl. Meteor.,* **10,** 674–683.

Taha, H., 1996: Modeling the impacts of increased urban vegetation on ozone air quality in the South Coast Air Basin. *Atmos. Environ.,* **30,** 3423–3430.

——, 1997: Modeling the impacts of large-scale albedo changes on ozone air quality in the South Coast Air Basin. *Atmos. Environ.,* **31,** 1667–1676.

——, 1999: Modifying a mesoscale meteorological model to better incorporate urban heat storage: A bulk-parameterization approach. *J. Appl. Meteor.,* **38,** 466–473.

Zehnder, J. A., 2002: Simple modifications to improve fifth-generation Pennsylvania State University–National Center for Atmospheric Research Mesoscale Model performance for the Phoenix, Arizona, metropolitan area. *J. Appl. Meteor.,* **41,** 971–979.